Electronic Supporting Information for

Universal Synthesis of Single-Atom Electrocatalysts *via In-Situ* Fluoride Ion Etching for Hydrogen Evolution

Peng Liu,[a] *Jiahui Ye,*[a] *Kuan Deng,*[a] *Xuesong Liu,*[a] *Haohui Dong,*[a] *He Zhang,*[a] *Wen Tian,*[a] *Junyi Ji*[a, b,]*

[a] School of Chemical Engineering, Sichuan University, Chengdu 610065, P. R. China

[b] State Key Laboratory of Polymer Materials Engineering, Sichuan University, Chengdu 610065, P. R. China

* Corresponding author. E-mail address

Junyi Ji, E-mail: junyiji@scu.edu.cn

Supplementary experimental section

1. Chemicals and materials

Carbon cloth (CC, W0S1011) was purchased from Suzhou Sinero Technology Co., Ltd. Ethanol (EtOH, AR), potassium permanganate ($KMnO_4$, AR), hydrochloric acid (HCl, AR), tetrabutyl titanate (TBT, AR), dicyandiamide (DCDA, AR) and ammonium fluoride (NH_4F, AR) were purchased from Chengdu Chron Chemical Co., Ltd. Potassium hydroxide (KOH, 85%), potassium chloride (KCl, 99.8%) and potassium fluoride (KF, 99.8%) were purchased from Aladdin. Ruthenium (III) trichloride trihydrate ($RuCl_3$ $3H_2O$, 99%), iridium (III) chloride trihydrate ($IrCl_3$ $3H_2O$, 98%), palladium (II) chloride ($PdCl_2$, 99%) and platinum (IV) chloride ($PtCl_4$, 97%) were purchased from Admas-Beta. All the raw chemicals and materials were used without purification.

2. Materials characterization

Scanning electron microscope (SEM, JEOL JMS-7610F) and transmission electron microscope (TEM, JEOL JEM-F200) were used for observing the surface morphology of the prepared materials. X-ray diffraction (XRD, SmartLab SE, Rigaku), energy dispersive spectroscopy (EDX) and X-ray photoelectron spectroscopy (XPS, PHI5000 Versa spectrometer) were used for determining the crystalline, elemental and valence state information of the sample, respectively. Laser Raman spectroscopy (Thermal Fisher DXR) was used to identify TiO_2 type. Electron paramagnetic resonance spectrometer (EPR, MS-5000X) was used to study the unpaired electronic states of samples.

3. Electrochemical measurements

The HER performances of prepared samples are measured in a standard three-electrode setup through a CHI 760E electrochemical workstation. F-M@TiO_xN_y (M = Ru, Pd, Ir, Pt) is directly used as working electrode. Hg/HgO and carbon rod were used as the reference electrode and counter electrode, respectively. 1 M KOH was used as electrolyte. LSV tests are carried out with a scan rate of 5 mV s^{-1} in the potential range of 0 to -1.7 V vs. Hg/HgO for HER. All the potentials mentioned in the figures were converted to potential versus reversible hydrogen electrode (vs. RHE) according to the Nernst equation:

$$E(\mathrm{RHE}) = E(\mathrm{Hg/HgO}) + 0.059\times\mathrm{pH} + 0.197$$

Chronopotentiometry tests are conducted at the current density of −10 mA cm^{-2} to evaluate the stability of the catalysts for HER. The electrochemical impedance spectroscopy was conducted at -0.844 and -1.004 V vs. Hg/HgO for HER, respectively, in the frequency range of 100 kHz to 0.1 Hz with an amplitude of 5 mV. The double layer capacitance (C_{dl}) was measured by collecting CV in the potential range of -0.3 to -0.2 V vs. Hg/HgO with various scan rates (10–50 mV s^{-1}) for HER. The electrochemically active surface area (ECSA) was calculated by taking the ratio of C_{dl} with specific capacitance C_{s} (40 μF cm^{-2} for a flat surface).

The TOF value is calculated by using the following formula:

$$\mathrm{N} = \frac{\mathrm{Q}}{2\mathrm{F}}$$

$$\mathrm{TOF}\left(\mathrm{s}^{-1}\right) = \frac{\mathrm{I}}{2\mathrm{NF}}$$

Where N is the amounts of the active sites, Q is the electric quantity, and I is the catalytic current. CV plot was recorded in a phosphate buffer solution at pH =7.4 from −0.2 V to 0.6 V vs. RHE with a scan rate of 50 mV s^{-1}.

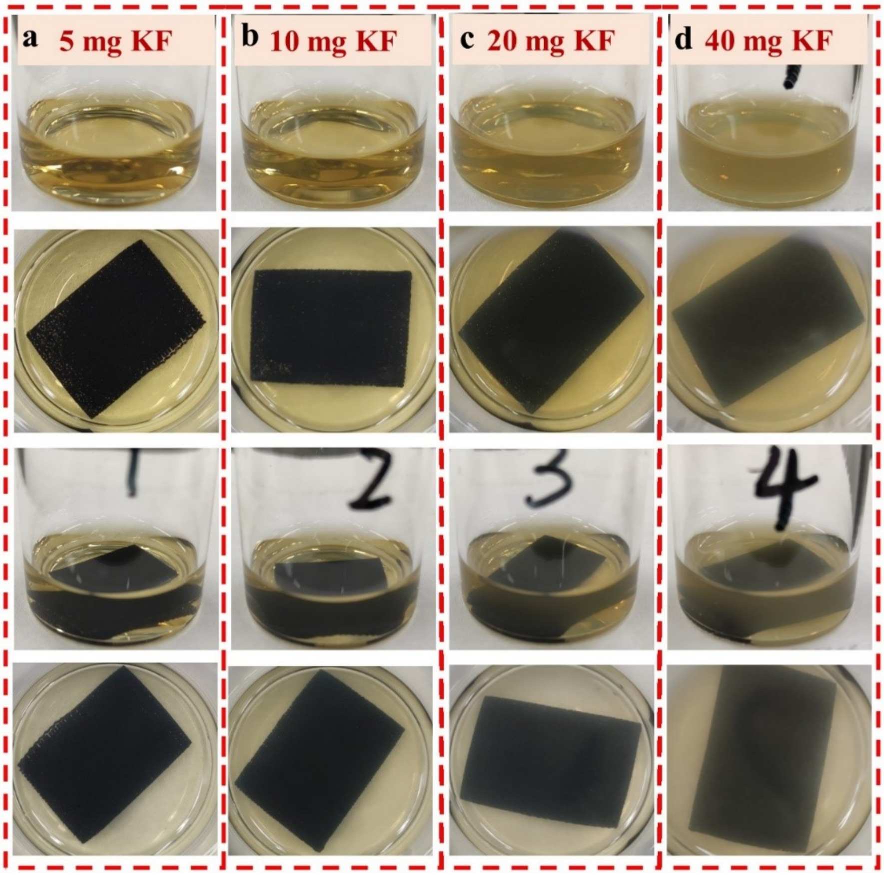

Figure S1. Photographs of the composites prepared under different KF addition amount: (a) F-Ru@TiO$_x$N$_y$-5, (b) F-Ru@TiO$_x$N$_y$-10, (c) F-Ru@TiO$_x$N$_y$-20 and (d) F-Ru@TiO$_x$N$_y$-40.

In order to determine the appropriate operating parameters, factors such as the type of salt, the type of carrier, the amount of KF, and the concentration of precious metals were investigated.

Firstly, different amounts of KF (5, 10, 20, and 40 mg) were investigated for the etching preparation of F-Ru@TiO$_x$N$_y$. As the dosage of KF increases, the solution becomes increasingly turbid (**Figure S1**), indicating that the F$^-$ etching process has become more drastic. Nevertheless, TiO$_x$N$_y$ retains its nanorod morphology (**Figure S2**). F-Ru@TiO$_x$N$_y$-10 demonstrates the best electrocatalytic hydrogen evolution performance, with an overpotential of 20.8 mV at a current density of 10 mA cm^{-2}, a Tafel slope of 59.9 mV dec^{-1}, the lowest internal resistance, and the highest electrochemical active surface area (ECSA) of 206.7 mF cm^{-2}. This indicates that the hydrogen evolution performance initially increases and then decreases with the amount of KF (**Figure S3, 4**). Therefore, the optimal amount of KF to be added is 10 mg.

Different concentrations of $RuCl_3$ $3H_2O$ (0.5, 1.0, 1.5, and 2.0 mM) were investigated for the preparation of Ru@TiO_xN_y. As the concentration of $RuCl_3$ $3H_2O$ increases, the solution becomes increasingly turbid (**Figure S5**), indicating fast F^- etching and Ru immobilization process. Nevertheless, TiO_xN_y still retains its nanorod morphology (**Figure S6**). F-Ru@TiO_xN_y-1.5 demonstrates the best electrocatalytic hydrogen evolution performance, with an overpotential of 20.8 mV at a current density of 10 mA cm^{-2}, a Tafel slope of 59.9 mV dec^{-1}, minimal internal resistance, and the largest electrochemical active surface area (ECSA) of 260.7 mF cm^{-2}. This indicates that the hydrogen evolution performance initially increases and then decreases with the concentration of $RuCl_3$ $3H_2O$ (**Figure S7, 8**). Therefore, the optimal concentration of $RuCl_3 \cdot 3H_2O$ is determined to be 1.5 mM.

Furthermore, Ru@TiO_xN_y prepared with various type of salts was investigated. The solution is clear with the presence of KCl (**Figure S9**), indicating that fluoride ions play an etching role. Additionally, TiO_xN_y retains its nanorod morphology (**Figure S10**). Meanwhile, although the electrocatalytic hydrogen evolution performance of the KF and NH_4F etched catalysts is similar, the former exhibits lower internal resistance and a greater electrochemical surface area (ECSA) (**Figure S11, 12**).

Further investigation was conducted on the changes in pH values before and after F^- etching the samples in the solution. Only in the absence of KF, the pH value of the etched solution increases, indicating an increase in hydroxide concentration after etching the sample with a mixed solution of ethanol and water. However, in the presence of 10 mg KF, there was no significant change in the pH value of the solution after F^- etching the sample (**Figure S13**). Therefore, it can be inferred that oxygen and hydrogen ions are generated during F^- etching process, and the reaction between hydrogen ions and hydroxide ions stabilizes the pH value of the etched solution.

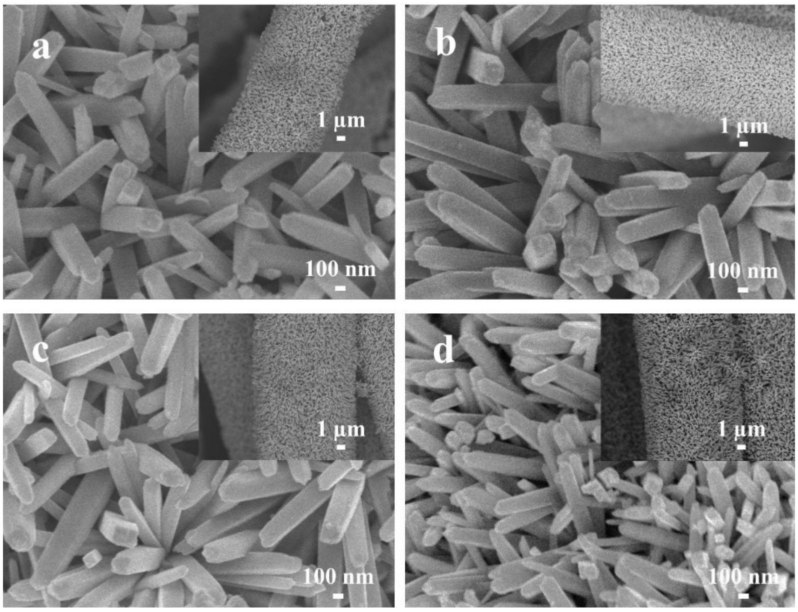

Figure S2. SEM images of (a) F-Ru@TiO$_x$N$_y$-5, (b) F-Ru@TiO$_x$N$_y$-10, (c) F-Ru@TiO$_x$N$_y$-20 and (d) F-Ru@TiO$_x$N$_y$-40.

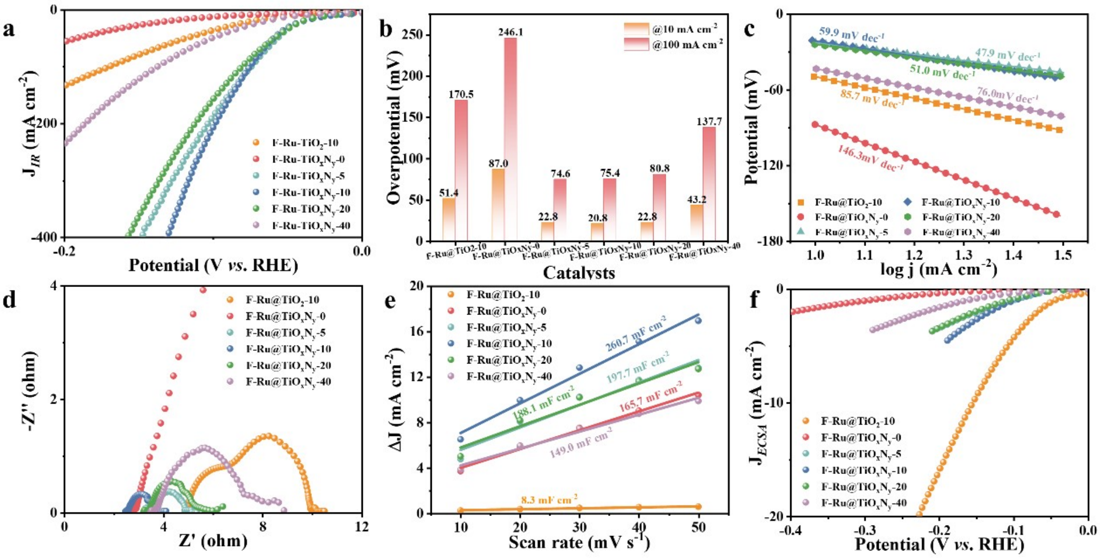

Figure S3. (a) LSV curves, (b) overpotential, (c) Tafel plots, (d) Nyquist plots, (e) ESCA and ECSA-normalized LSV curves of F-Ru@TiO$_2$-10, F-Ru@TiO$_x$N$_y$-0, F-Ru@TiO$_x$N$_y$-5, F-Ru@TiO$_x$N$_y$-10, F-Ru@TiO$_x$N$_y$-20 and F-Ru@TiO$_x$N$_y$-40.

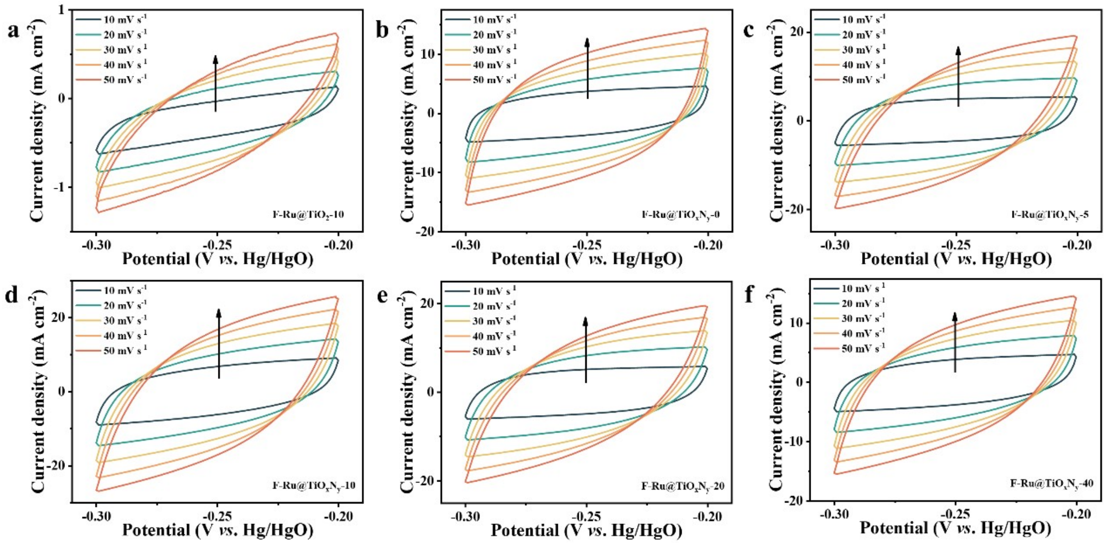

Figure S4. CV curves of the F-Ru@TiO_2-10, F-Ru@TiO_xN_y-0, F-Ru@TiO_xN_y-5, F-Ru@TiO_xN_y-10, F-Ru@TiO_xN_y-20 and F-Ru@TiO_xN_y-40.

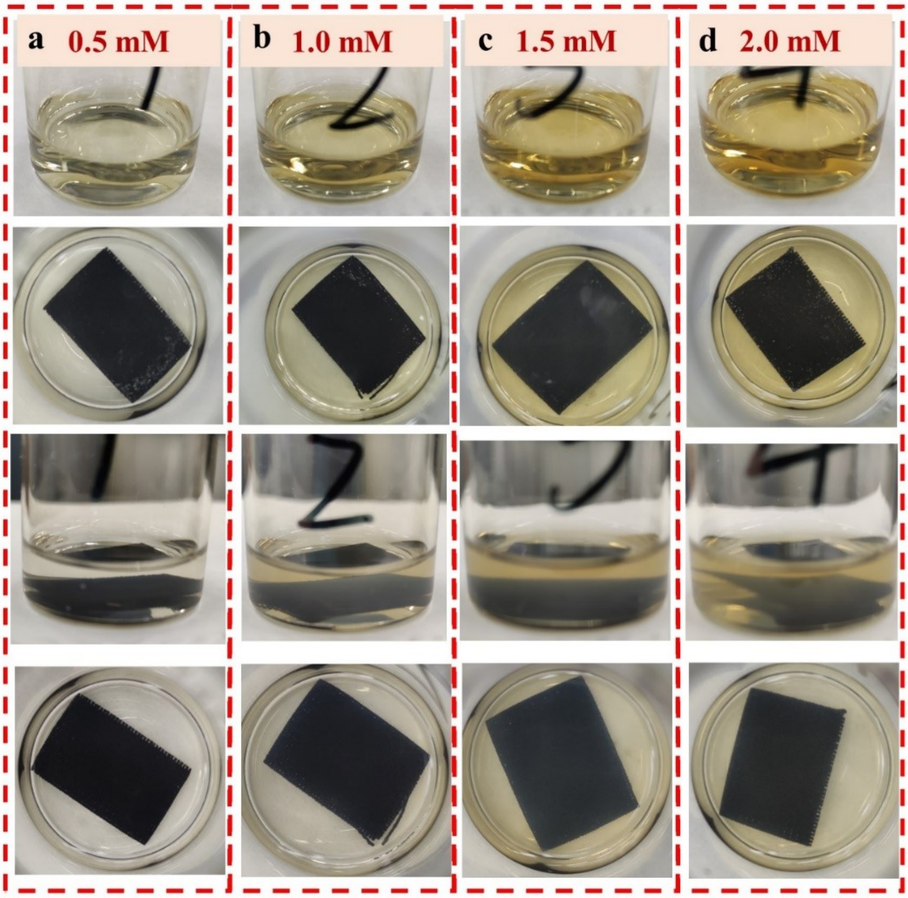

Figure S5. Photographs of the composites prepared under different Ru addition dosage: (a) F-Ru@TiO_xN_y-0.5, (b) F-Ru@TiO_xN_y-1, (c) F-Ru@TiO_xN_y-1.5 and (d) F-Ru@TiO_xN_y-2.

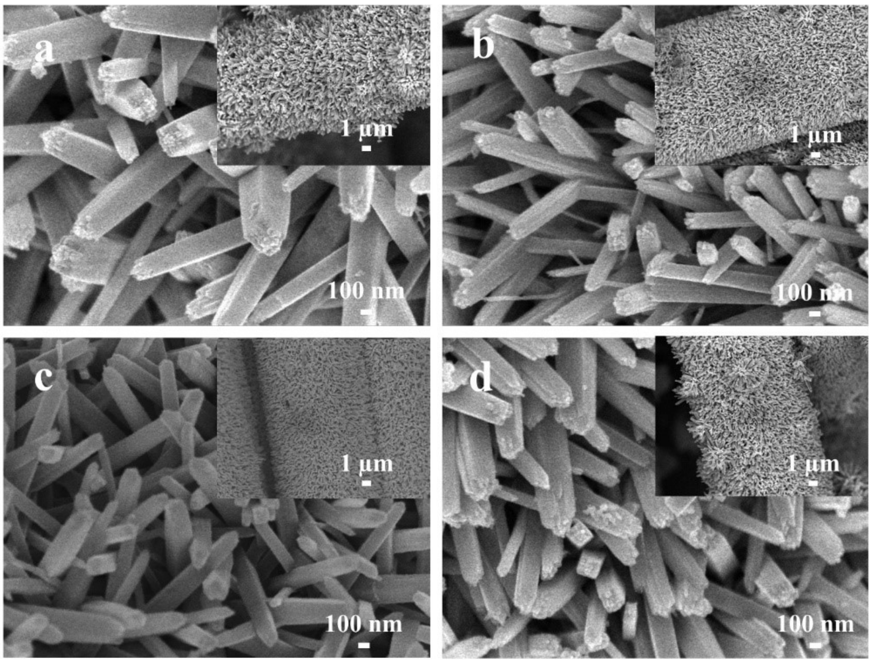

Figure S6. SEM images of (a) F-Ru@TiO_xN_y-0.5, (b) F-Ru@TiO_xN_y-1, (c) F-Ru@TiO_xN_y-1.5 and (d) F-Ru@TiO_xN_y-2.

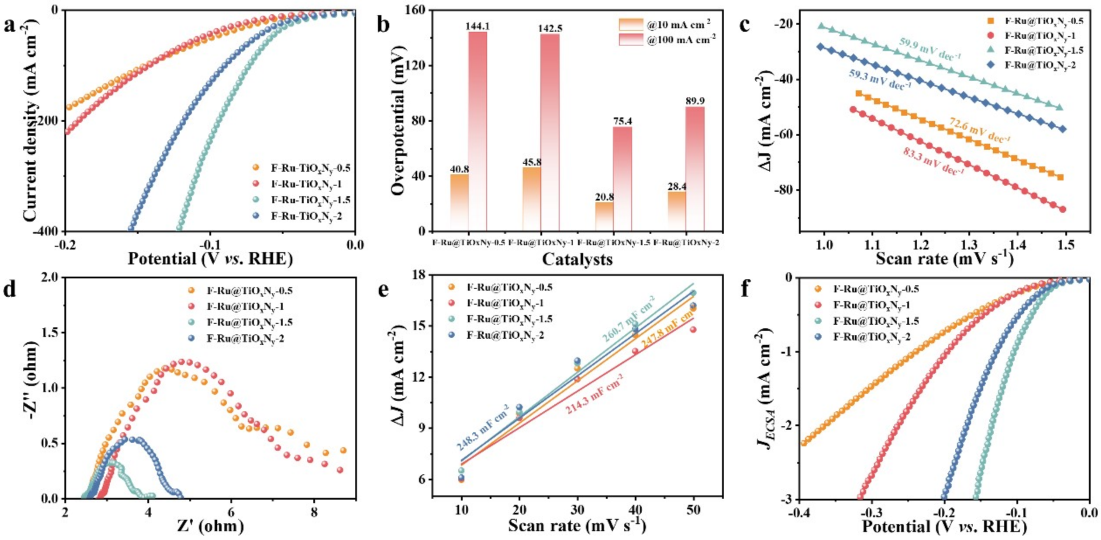

Figure S7. (a) LSV curves, (b) overpotential, (c) Tafel plots, (d) Nyquist plots, (e) ESCA and ECSA-normalized LSV curves of F-Ru@TiO$_x$N$_y$-0.5, F-Ru@TiO$_x$N$_y$-1, F-Ru@TiO$_x$N$_y$-1.5 and F-Ru@TiO$_x$N$_y$-2.

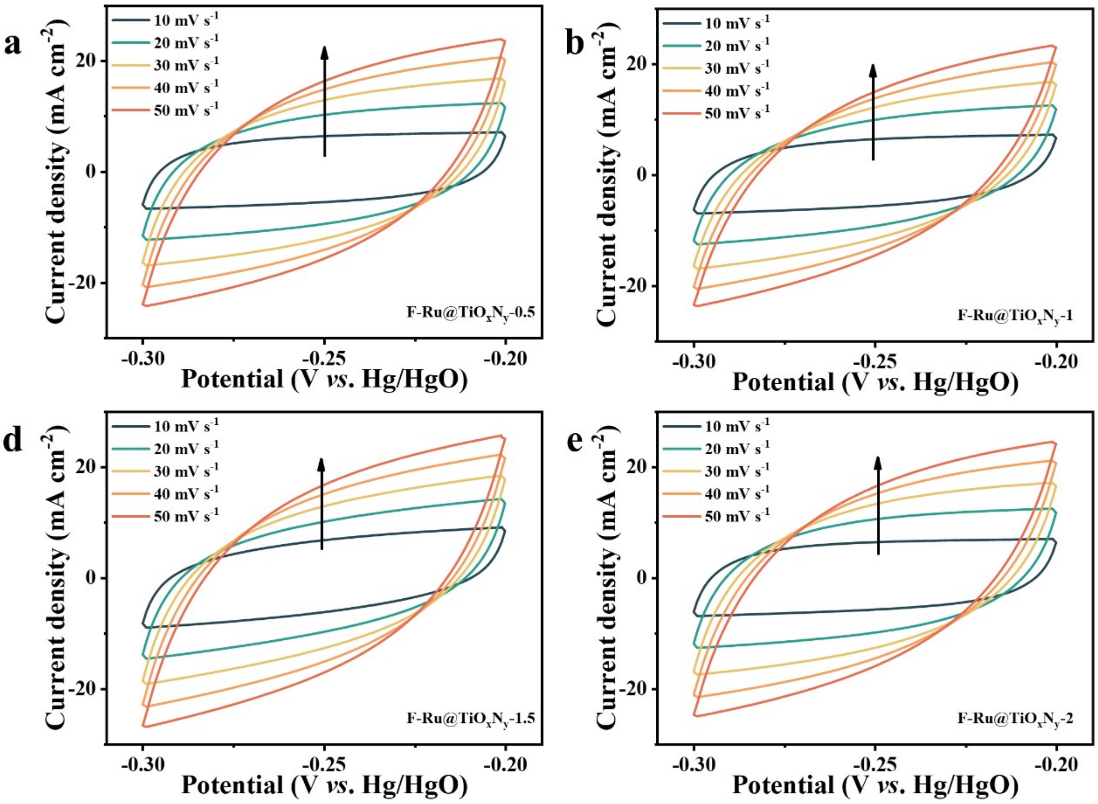

Figure S8. CV curves of (a) F-Ru@TiO$_x$N$_y$-0.5, (b) F-Ru@TiO$_x$N$_y$-1, (c) F-Ru@TiO$_x$N$_y$-1.5 and (d) F-Ru@TiO$_x$N$_y$-2.

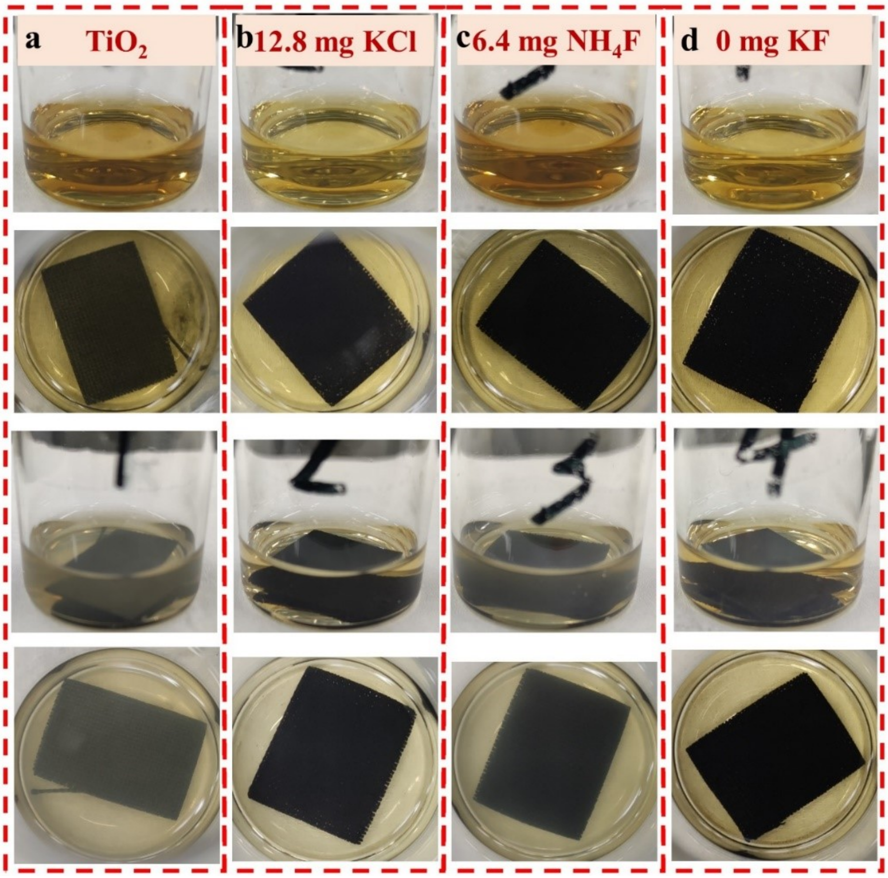

Figure S9. Photographs of the composites prepared under different etchant agents: (a) TiO_2-10 mg KF, (b) TiO_xN_y-12.8 mg KCl, (c) TiO_xN_y-6.4 mg NH_4F and (d) TiO_xN_y-0 mg KF.

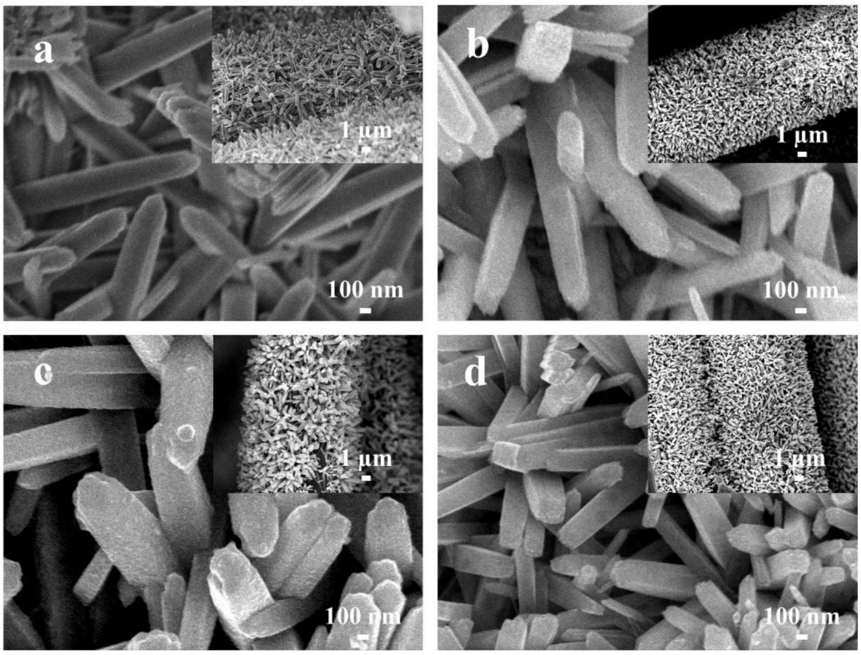

Figure S10. SEM images of (a) Ru@TiO_2, (b) Ru@TiO_xN_y-KCl, (c) Ru@TiO_xN_y-NH_4F and (d) Ru@TiO_xN_y-KF.

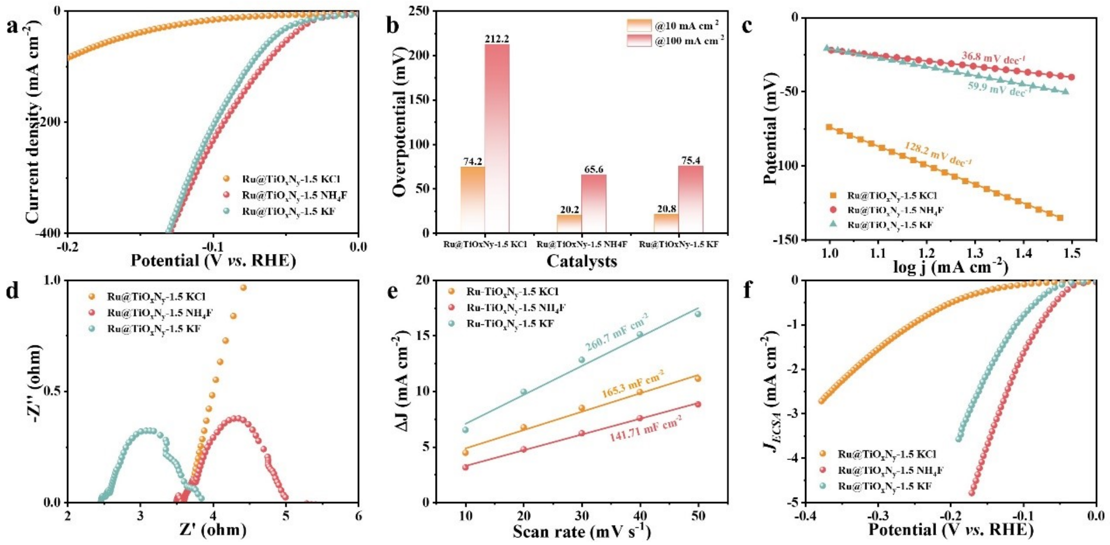

Figure S11. (a) LSV curves, (b) overpotential, (c) Tafel plots, (d) Nyquist plots, (e) ESCA and ECSA-normalized LSV curves of Ru@TiO$_x$N$_y$-KCl, Ru@TiO$_x$N$_y$-NH$_4$F and Ru@TiO$_x$N$_y$-KF.

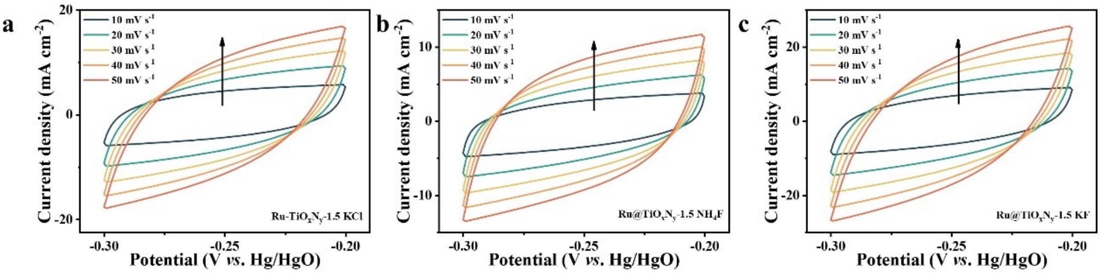

Figure S12. CV curves of the (a) Ru@TiO$_x$N$_y$-KCl, (b) Ru@TiO$_x$N$_y$-NH$_4$F and (c) Ru@TiO$_x$N$_y$-KF under different scan rates.

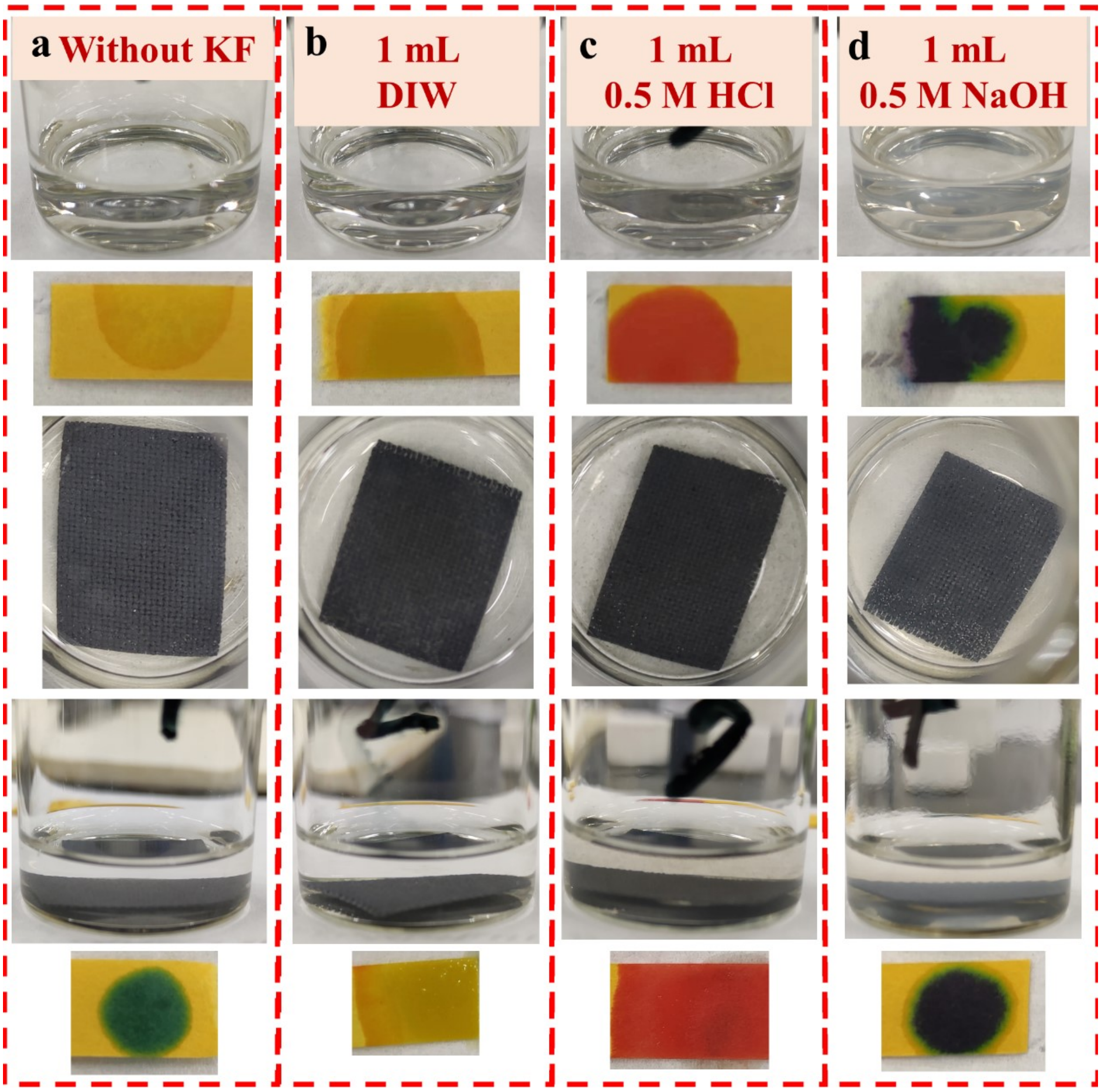

Figure S13. Photographs of the composites prepared under different solution conditions: (a) without KF, (b) 1 mL DI W, (c) 1 mL 0.5 M HCl and (d) 1 mL 0.5 M KOH.

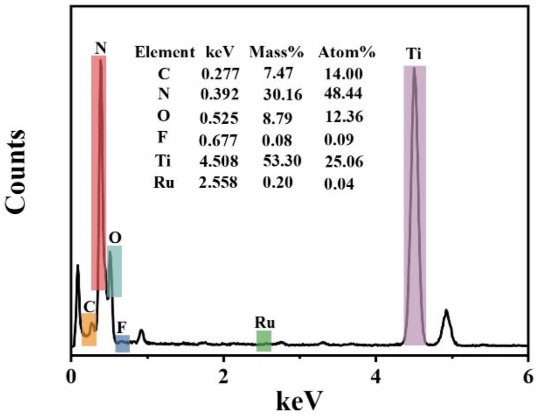

Element	keV	Mass%	Atom%
C	0.277	7.47	14.00
N	0.392	30.16	48.44
O	0.525	8.79	12.36
F	0.677	0.08	0.09
Ti	4.508	53.30	25.06
Ru	2.558	0.20	0.04

Figure S14 EDX spectrum of Ru@TiO$_x$N$_y$.

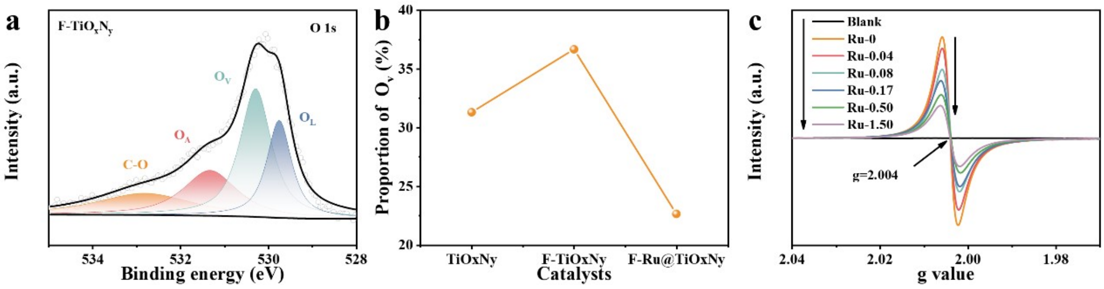

Figure S15 (a) O 1s spectra of the F-TiO$_x$N$_y$. (c) Proportion of O$_v$ in different catalysts. (c) Relationship between peak intensity of oxygen vacancies and Ru concentration of the F-Ru@ TiO$_x$N$_y$.

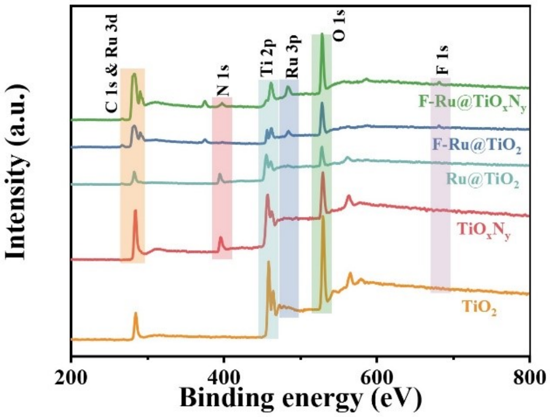

Figure S16 XPS full survey spectra of the as-prepared composites.

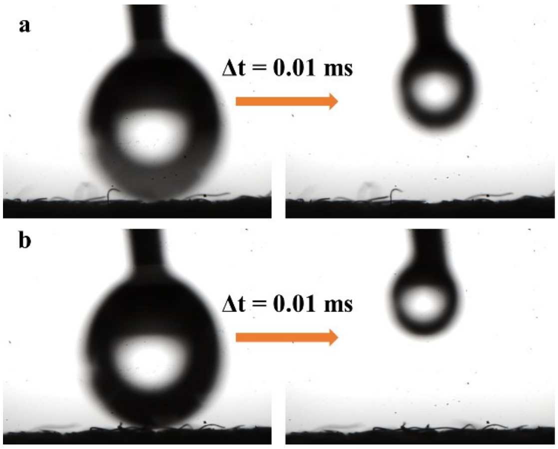

Figure S17. Static water contact angles of (a) F-Ru@TiO_xN_y and (b) TiO_xN_y.

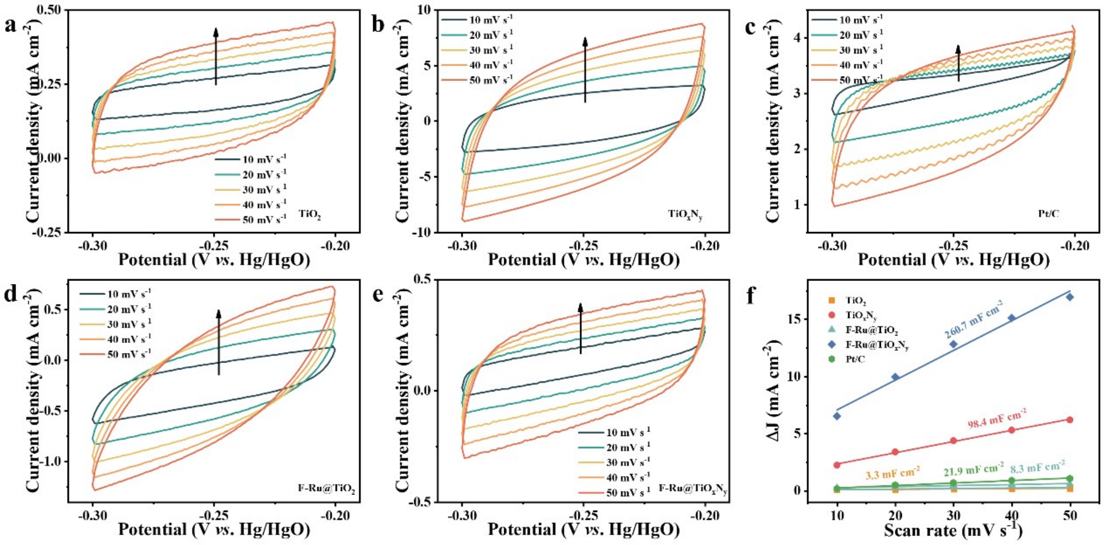

Figure S18. CV curves of (a) TiO_2, (b) TiO_xN_y, (c) Pt/C, (d) F-Ru@TiO_2 and (e) F-Ru@TiO_xN_y. (f) Calculated ECSA values.

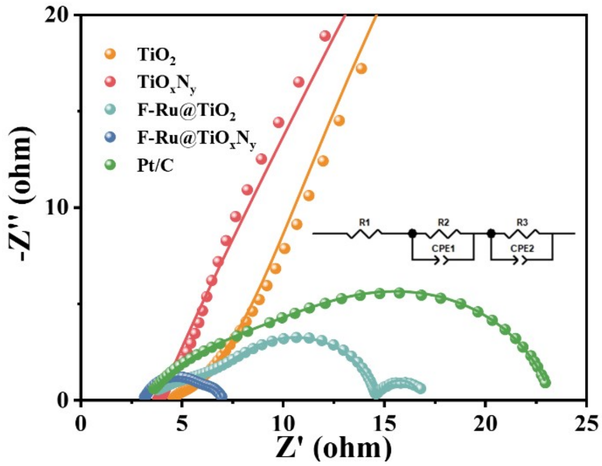

Figure S19 Nyquist plots of the as-prepared electrodes.

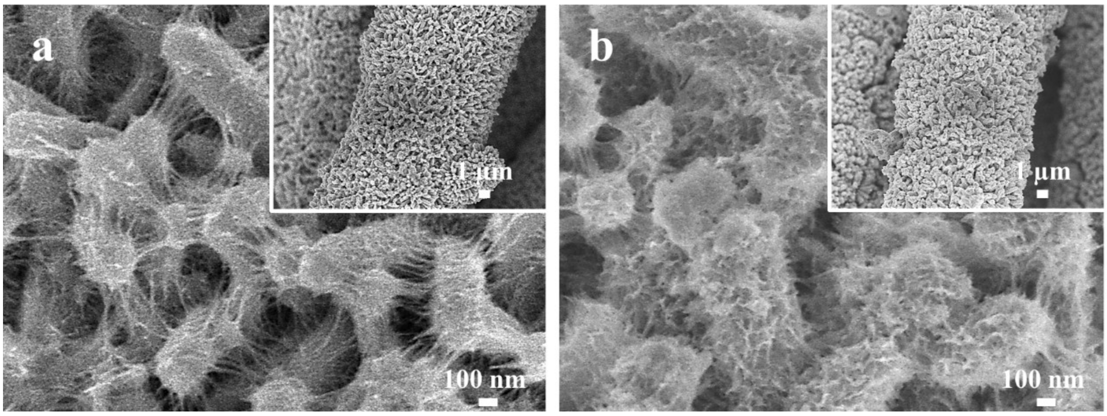

Figure S20 SEM images of the F-Ru@TiO$_x$N$_y$ after long-term test for (a) 24 h at 10 mA cm^{-2} and (b) 48 h at 100 mA cm^{-2}.

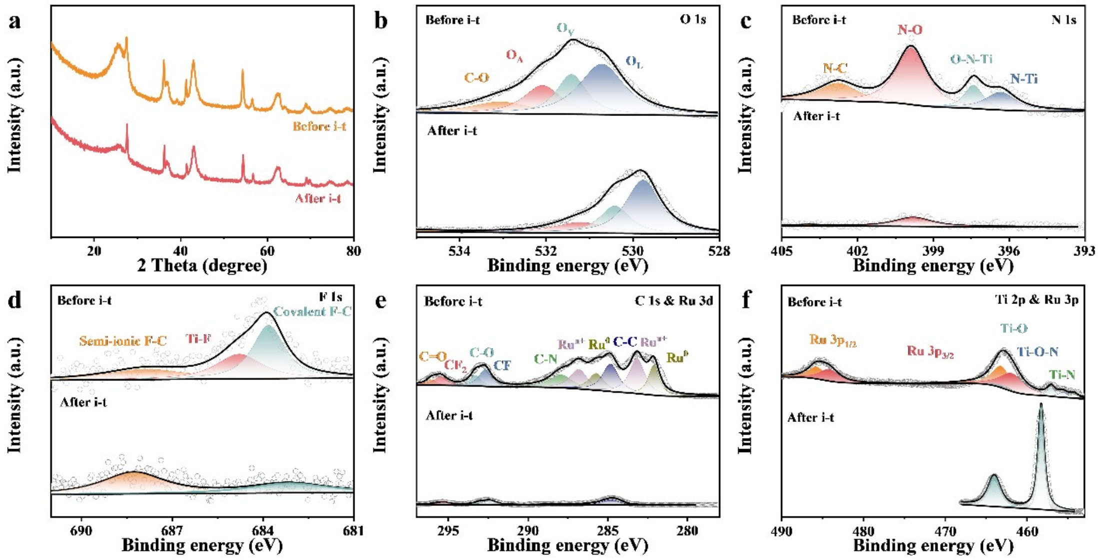

Figure S21 (a) XRD patterns after and before long-term test for 48 h at 100 mA cm^{-2}. XPS spectra of the (b) O 1s, (c) N 1s, (d) F 1s, (e) C 1s & Ru 3d and (f) Ti 2p & Ru 3p after and before 48 h long-term test at 100 mA cm^{-2}.

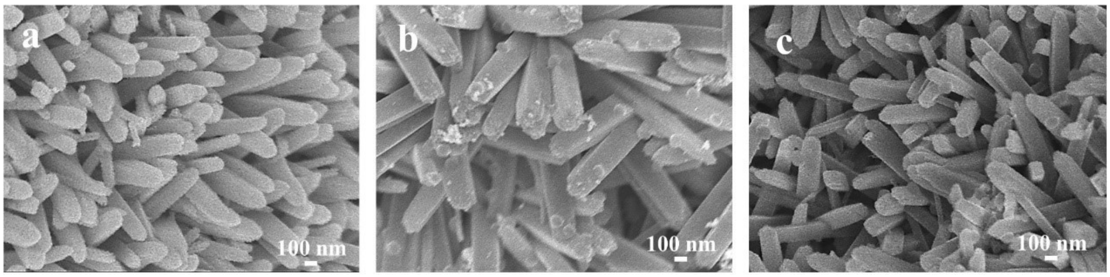

Figure S22. SEM images of (a) F-Pd@TiO_xN_y, (b) F-Ir@TiO_xN_y and (c) F-Pt@TiO_xN_y.

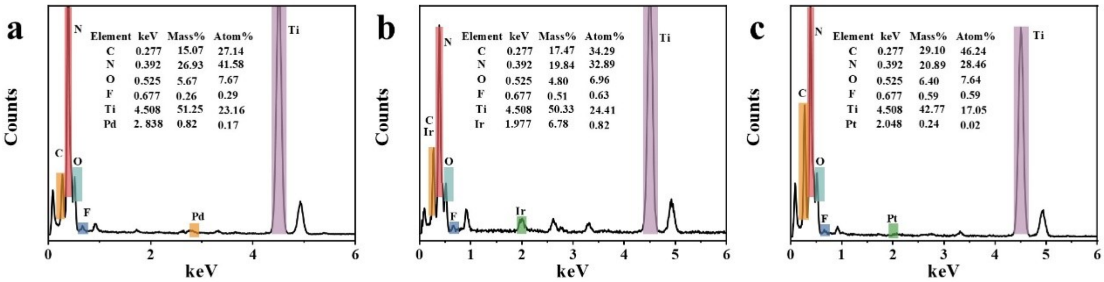

Element	keV	Mass%	Atom%
C	0.277	15.07	27.14
N	0.392	26.93	41.58
O	0.525	5.67	7.67
F	0.677	0.26	0.29
Ti	4.508	51.25	23.16
Pd	2. 838	0.82	0.17

Element	keV	Mass%	Atom%
C	0.277	17.47	34.29
N	0.392	19.84	32.89
O	0.525	4.80	6.96
F	0.677	0.51	0.63
Ti	4.508	50.33	24.41
Ir	1.977	6.78	0.82

Element	keV	Mass%	Atom%
C	0.277	29.10	46.24
N	0.392	20.89	28.46
O	0.525	6.40	7.64
F	0.677	0.59	0.59
Ti	4.508	42.77	17.05
Pt	2.048	0.24	0.02

Figure S23. EDX of (a) F-Pd@TiO$_x$N$_y$, (b) F-Ir@TiO$_x$N$_y$ and (c) F-Pt@TiO$_x$N$_y$.

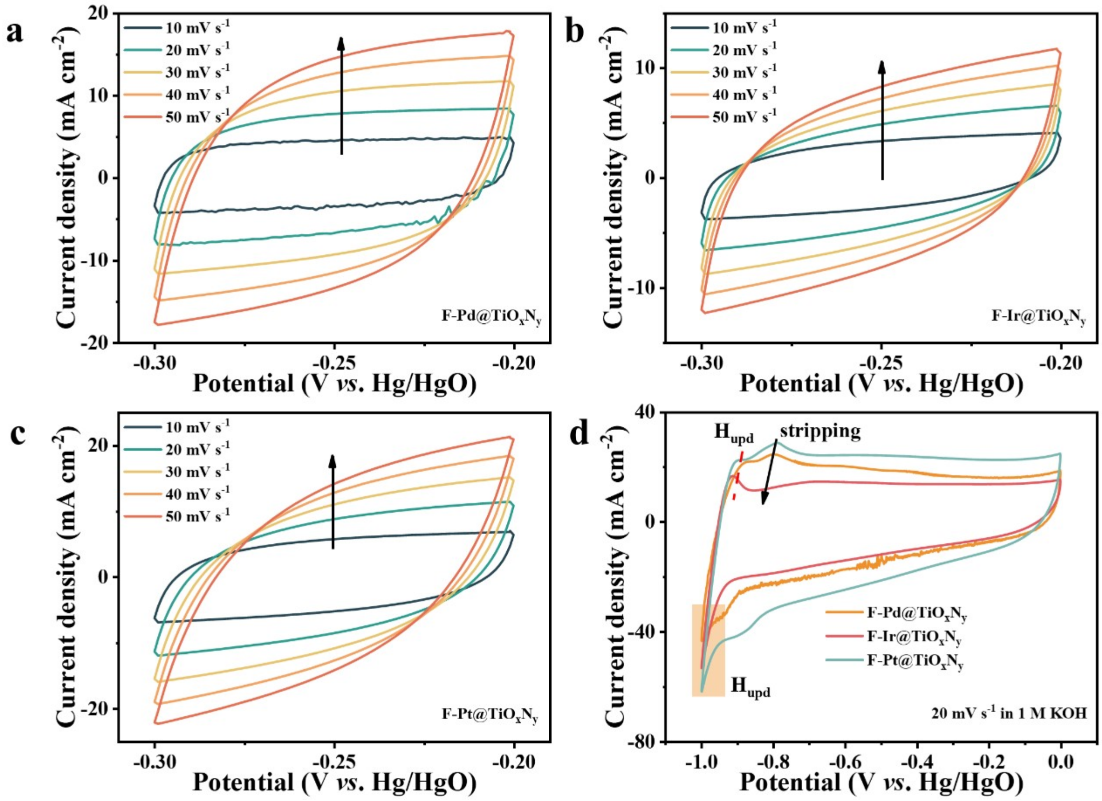

Figure S24. CV curves of (a) F-Pd@TiO_xN_y, (b) F-Ir@TiO_xN_y and (c) F-Pt@TiO_xN_y. (d) CV curves of F-Pd@TiO_xN_y, F-Ir@TiO_xN_y and F-Pt@TiO_xN_y at 20 mV s^{-1} from -1.0–0 V.

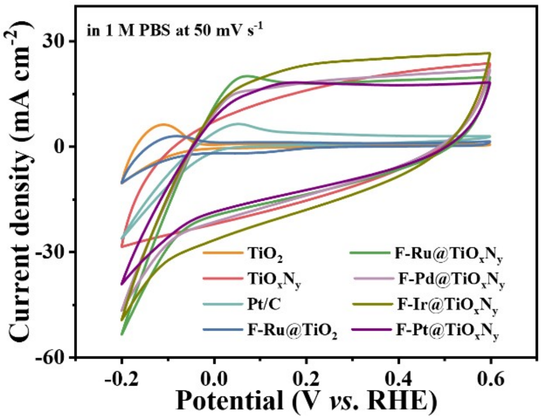

Figure S25. Cyclic voltammetry (CV) curves recorded in a phosphate buffer solution.

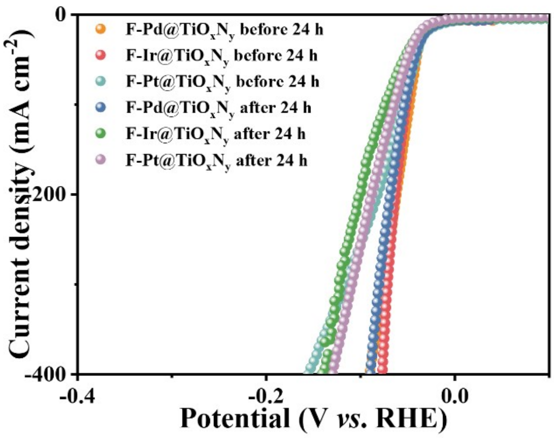

Figure S26. LSV curves of F-Pd@TiO$_x$N$_y$, F-Ir@TiO$_x$N$_y$ and F-Pt@TiO$_x$N$_y$ before/after 24 h test at constant potential around 100 mA cm^{-2}.

Table S1. HER performances comparison of recently reported representative electrocatalysts in alkaline medium.

Materials	Overpotentials @10 mA cm^{-2} (mV)	Tafel (mV dec^{-1})	Stability	Ref.
Ru@TiO$_x$N$_y$	20.8	59.9	48 h@100 mA cm^{-2}	**this work**
Pd@TiO$_x$N$_y$	27.2	56.7	24 h@100 mA cm^{-2}	**this work**
Ir@TiO$_x$N$_y$	13.2	48.6	24 h@100 mA cm^{-2}	**this work**
Pt@TiO$_x$N$_y$	12.8	40.2	24 h@100 mA cm^{-2}	**this work**
Ru/r-TiO$_2$	15	49	10 h@10 mA cm^{-2}	[1]
Ru MIs-MoS$_2$	17	63	—	[2]
LaCeO$_x$@NGr/Ru$_1$	22	44	30 h@20 mA cm^{-2}	[3]
NiRu$_{0.13}$-BDC	34	32	—	[4]
RuP$_4$@CoP/Ti	36	54.8	12 h@10 mA cm^{-2}	[5]
Ru/TiN-300	38	39	24 h@10 mA cm^{-2}	[6]
Ru@N-TiO$_2$/C	39	47	10 h@10 mA cm^{-2}	[7]
Ru-TiO/TiO$_2$@NC	39	49	24 h@25 mA cm^{-2}	[8]
RTN20	43	56	40 h@10 mA cm$_{-2}$	[9]
Ru–CrN/NC	53	59	24 h@10 mA cm^{-2}	[10]
Ru@TiO$_2$	57	67	12 h@10 mA cm^{-2}	[11]
Ru$_{0.33}$Se@TNA	57	50	10 h@10 mA cm^{-2}	[12]
RuS$_x$/S–GO	58	56	12 h@50 mA cm^{-2}	[13]
Ru@TiO$_2$	62	70	12 h@10 mA cm^{-2}	[14]
Ru-RuO$_2$@NPC	90	68	9 h@10 mA cm^{-2}	[15]
R-TiO$_2$:Ru (5%)	113	95	—	[16]

References

1. L.-N. Chen, S.-H. Wang, P.-Y. Zhang, Z.-X. Chen, X. Lin, H.-J. Yang, T. Sheng, W.-F. Lin, N. Tian, S.-G. Sun and Z.-Y. Zhou, *Nano Energy*, 2021, **88**, 106211.
2. X. Li, S. Han, Z. Qiao, X. Zeng, D. Cao and J. Chen, *Chem. Eng. J.*, 2023, **453**, 139803.
3. V. Dao, H. Choi, S. Yadav, J. D. Jiménez, C. Kim, T. Van Nguyen, K. Chen, P. Uthirakumar, Q. Van Le, S. D. Senanayake, H. Y. Kim and I.-H. Lee, *Appl. Catal. B Environ.*, 2024, **343**, 123452.
4. Y. Sun, Z. Xue, Q. Liu, Y. Jia, Y. Li, K. Liu, Y. Lin, M. Liu, G. Li and C.-Y. Su, *Nat. Commun.*, 2021, **12**, 1369.
5. W. Wang, H. Zhao, Y. Du, Y. Yang, Y. Liu and L. Wang, *Appl. Surf. Sci.*, 2020, **534**, 147626.
6. X. Wang, X. Yang, G. Pei, J. Yang, J. Liu, F. Zhao, F. Jin, W. Jiang, H. Ben and L. Zhang, *Carbon Energy*, 2024, **6**, e391.
7. W. Xu, H. Xie, F. Cao, S. Ran, Y. Duan, B. Li and L. Wang, *J. Mater. Chem. A*, 2022, **10**, 23751-23759.
8. L. Jing, G. Jie, W. Yu, H. Ren, X. Cui, X. Chen and L. Jiang, *Chem. Eng. J.*, 2023, **472**, 145009.
9. S. Y. Yun, S. Lee, X. Jin, A. Soon and S.-J. Hwang, *Adv. Sci.*, 2024, **11**, 2309819.
10. B. Sarkar, B. K. Barman, A. Parui, A. K. Singh and K. K. Nanda, *J. Mater. Chem. A*, 2024, **12**, 8291-8301.
11. S. Liang, C. Dong, C. Zhou, R. Wang and F. Huang, *Nano Lett.*, 2024, **24**, 757-763.
12. K. Wang, Q. Chen, Y. Hu, W. Wei, S. Wang, Q. Shen and P. Qu, *Small*, 2018, **14**, 1802132.
13. P. Li, X. Duan, S. Wang, L. Zheng, Y. Li, H. Duan, Y. Kuang and X. Sun, *Small*, 2019, **15**, 1904043.
14. Y. Cao, S. Liang, Y. Yan, W. Dong, C. Dong, W. Zheng, S. Nong and F. Huang, *Inorg. Chem. Front.*, 2023, **10**, 3852-3859.
15. N. Wang, S. Ning, X. Yu, D. Chen, Z. Li, J. Xu, H. Meng, D. Zhao, L. Li, Q. Liu, B. Lu and S. Chen, *Appl. Catal. B Environ.*, 2022, **302**, 120838.
16. S. Nong, W. Dong, J. Yin, B. Dong, Y. Lu, X. Yuan, X. Wang, K. Bu, M. Chen, S. Jiang, L.-M. Liu, M. Sui and F. Huang, *J. Am. Chem. Soc.*, 2018, **140**, 5719-5727.